SuperEMFL

Superconducting magnets
for the European Magnet Field Laboratory

Grant Agreement n° 951714
Research and Innovation Action

Deliverable D3.3 Functional Material properties

Start date of the project: 1st January 2021

Duration: 48 months

Project Coordinator: Xavier Chaud – CNRS LNCMI (P1 - CNRS)

Contact: xavier.chaud@lncmi.cnrs.fr

This project has received funding from the European Union's Horizon 2020 research and innovation programme under grant agreement No 951714. Any dissemination of results must indicate that it reflects only the author's view and that the Commission is not responsible for any use that may be made of the information it contains.

Document Classification

Title	Functional Material properties
Deliverable	D3.3
Reporting Period:	RP2
Date of Delivery foreseen in DoA	Project Month 36 – 31 12 2023
Actual Date of Delivery to EC	Project Month 50 – 25 02 2025

Authors	Marc Dhallé P07 - UT
Work package	WP3 Materials testing
Dissemination	**PU = Public, fully open, e.g. web**
Type	R: Document, report
Version	*V*1
Doc ID Code	D3.3_SuperEMFL_P07_UT_250224
Keywords	Report

Document History

Partner	Remark	Version	Date
P07 UT	Final version	V1	24 02 2025

Document Validation

Partner	Approval (Signature or e-mail reference)
P07 UT	m.m.j.dhalle@utwente.nl
P01_CNRS	Xavier CHAUD

Document Abstract

D3.3 reports on the activities in Task 3.2 "*Functional materials testing*" within WP3 "*Materials Testing*".

This task was foreseen in support of the modelling efforts within WP4 "*Magnet Design*", and its detailed scope was deliberately left open in the project's Grant Agreement, to be defined as the needs for specific input became clear.

Since the properties of the envisaged structural materials are sufficiently well documented in earlier literature, the main uncertainty was identified to be in the thermal- and mechanical properties of the tapes used in the winding pack themselves. Recent thermal data were found in literature, so that the efforts in Task 3.2 were focused on the mechanical behavior of the tapes used in the coils of WP3 and WP5.

Section 3 of this report describes the set-up that was adapted at UT to handle the tape materials used in the project and to characterize them in terms of stress-strain and critical current density vs strain. The results of this characterization campaign is also described.

Abbreviations

E:	Young's modulus
ε:	axial strain
ε_{irr}:	maximum strain supported before irreversible degradation sets in
HTS:	High Temperature Superconductor
I_c:	maximum current level supported without significant ohmic dissipation
J_c:	maximum current density supported without significant ohmic dissipation
n:	factor describing steepness of superconducting-to-normal transition
ReBCO:	Rare earth Barium Copper Oxide
Rp0.2:	yield stress
σ:	axial stress
σ_{irr}:	maximum stress supported before irreversible degradation sets in
TARSIS:	Test ARrangement for Strain Influence on Strands

Contents

1. Introduction 5
2. Thermal properties of HTS tape material 5
3. Mechanical properties of HTS tape material 6
   3.1 Introduction 6
   3.2 Experimental details 6
   3.3 Results 10
4. Sources 15

1. Introduction

In the preparation phase of the SuperEMFL project, Task 3.2 "*Functional materials testing"* was foreseen in order to "*… (support) magnet design WP4 (by employing) the specialized characterization infrastructure that is available throughout the consortium to qualify materials and feed their properties back into WP4.The outcome of this task will be a measurements report (deliverable D23) clarifying the critical properties of the various functional materials that are selected.*" (SuperEMFL Grant Agreement).

Midway the project, the main such needs were identified by the actors in WP4 as **1)** the thermal properties of the HTS tapes themselves, needed as input for the thermal modeling (in especially thermal stability and quench development); and **2)** the mechanical characterization of the tape material (for comparison with calculated stress levels of various designs and thus as an indication of mechanical feasibility). Functional materials other that the tape windings themselves (metal reinforcement structures; polymer insulation etc.) were deemed sufficiently well documented by earlier literature.

For the thermal tape properties, a literature review turned up a recent and extensive database of the thermal conductivity and expansion coefficients from tape materials produced worldwide, compiled by Beijing University (see section 2 below). Since also the producers that are used for coil production in SuperEMFL were included, the consortium decided not to carry out similar studies but to use these literature data instead.

The need for mechanical characterization of the tape material used in SuperEMFL was met by University of Twente, that upgraded one of its existing stress-strain set-ups to allow for critical current characterization under the same conditions. This upgraded set-up and the results obtained with it on SuperEMFL's tape material are described in section 3 of this report.

2. Thermal properties of HTS tape material

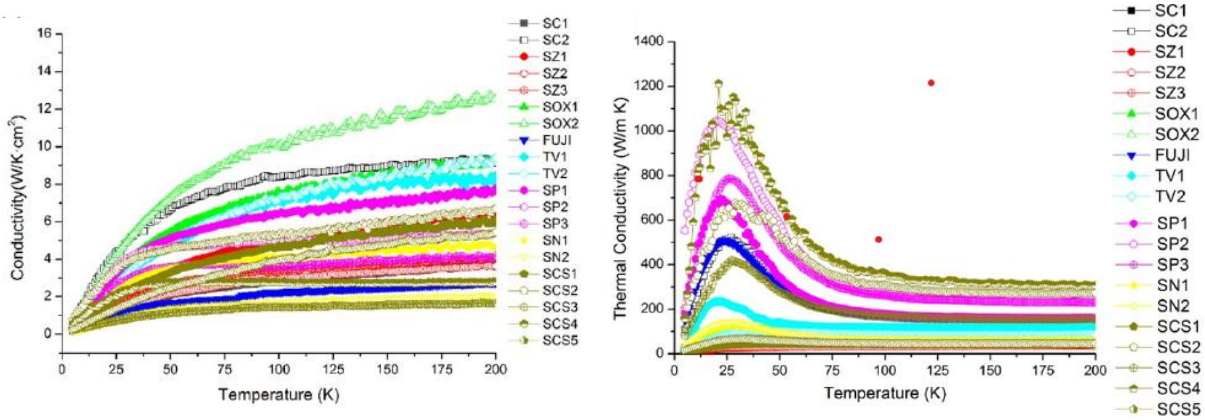

Figure 2.1: *Temperature dependence of the thermal conductivity of a wide range of ReBCO tapes in the transverse (left plot) and axial direction (right plot) . Compiled from literature [1].*

Figure 2.1 shows an example of the temperature-dependent data on thermal tape properties in the comprehensive data base compiled at Beijing University of Technology [1,2]. Since these data fulfilled the immediate needs for input in the model calculations of CEA and IEE within WP4, it was decided to direct further characterization efforts within SuperEMFL on the mechanical properties of the tapes used in WP3 and WP5.

3. Mechanical properties of HTS tape material

3.1 Introduction

Samples from the various tapes that were used by CNRS and Noell in Task 3.4 '*Small-scale model coil manufacture*' (see also deliverable reports D3.2 and D3.4) were characterized at the University of Twente in terms of their critical current I_c as a function of applied axial tensile stress σ; as well as in terms of their axial stress-strain σ - ε response.

For ease of reference, the key results derived from these tests are reported in Table 3.1 below. Experimental details and more detailed test results are reported in sections 3.2 and 3.3, respectively.

Table 3.1. *Key mechanical data of the tested samples: Young's modulus E; yield stress Rp0.2; unloaded critical current density J_c (at T=77K, self-field) ; corresponding n-value of the superconducting transition; irreversible strain limit ε_{irr};for J_c degradation; and corresponding irreversible stress limit σ_{irr}.*

Sample	*E* [GPa]	*Rp0.2* [MPa]	J_c [A/mm^2]	*n* [-]	ε_{irr} [%]	σ_{irr} [MPa]
THEVA 220057	191	1060	430	26	n.a.	n.a.
THEVA 230039	193	1160	523	35	0.28	440
THEVA 240019	189	1080	421	33	0.29	500
Fujikura 22-0197-03	147	786	676	28	0.39	570
SSTC 2311-351	180	1160	599	34	0.42	680
SSTC 2402-1911	177	974	639	34	0.36	570

$J_c(\varepsilon)$ and $\sigma(\varepsilon)$ data were ideally obtained on two different samples from the same tape. For some tapes (see section 3.3), not enough material length was left after the coil-winding of Task 3.4. For these, both experiments were done on the same sample, first $J_c(\varepsilon)$ and then $\sigma(\varepsilon)$. Hence, these $\sigma(\varepsilon)$ data do not correspond to a 'virgin' sample, but rather a sample already exposed to a strain level $\varepsilon \approx 0.4 - 0.5\%$ (and thus likely somewhat work-hardened). Also the possible influence of the laser-cutting on the mechanical properties is still somewhat debated[1]. For these reasons, UT and THEVA agreed to extend the collaboration beyond the duration of project, with sufficient length of THEVA's 4mm-wide high-pinning material furnished to be tested on multiple samples and without laser-cutting.

3.2 Experimental details

Tapes were tested in the TARSIS (Test ARrangement for Strain Influence on Strands) facility at UT. A schematic of the setup is shown in Figure 3.1. The TARSIS facility applies axial stress and strain on a ReBCO sample submerged in liquid nitrogen. Current leads and voltage taps are present to determine the critical current of the sample under this applied load.

[1] Un-loaded J_c and *n*-values were verified to be the same before and after laser-cutting, but a possible influence if the cutting on the ε_{irr} and σ_{irr} values themselves – due tot he modification of the sample edges - can at present not be fully excluded.

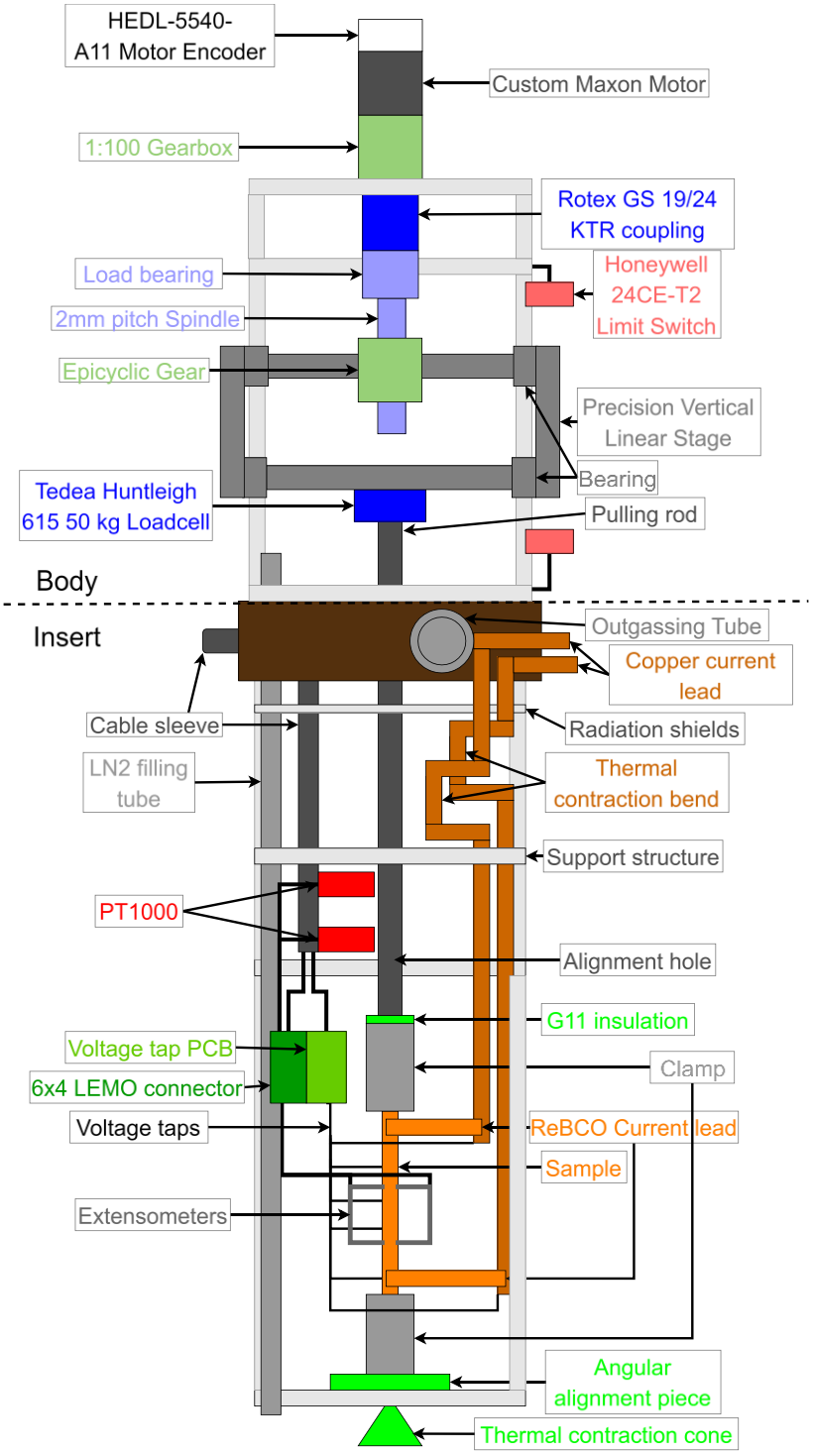

Figure 3.1: Schematic overview of The TARSIS test facility (Copper clamp current leads not shown).

To ensure that the measured superconducting-to-normal transition occurs in the region monitored by the voltage taps and the extensometer, samples were laser-cut into a dog-bone shape, shown in Figure 3.2 and 3.3. Without this 'necking' step, current-entrance effects and stress concentration caused by the clamps systematically caused the 6mm-wide samples to quench in the vicinity of the current leads[2]. The dog-bone shape allows for reliable results.

[2] TARSIS was designed to handle 4mm-wide material and operate at corrspondingly lower currents. The critical current levels of the 6mm wide tapes lead to excessive heating (and uncontrolled, thermally driven transitions) near the clamps well before the central – monitored – section reached its I_c.

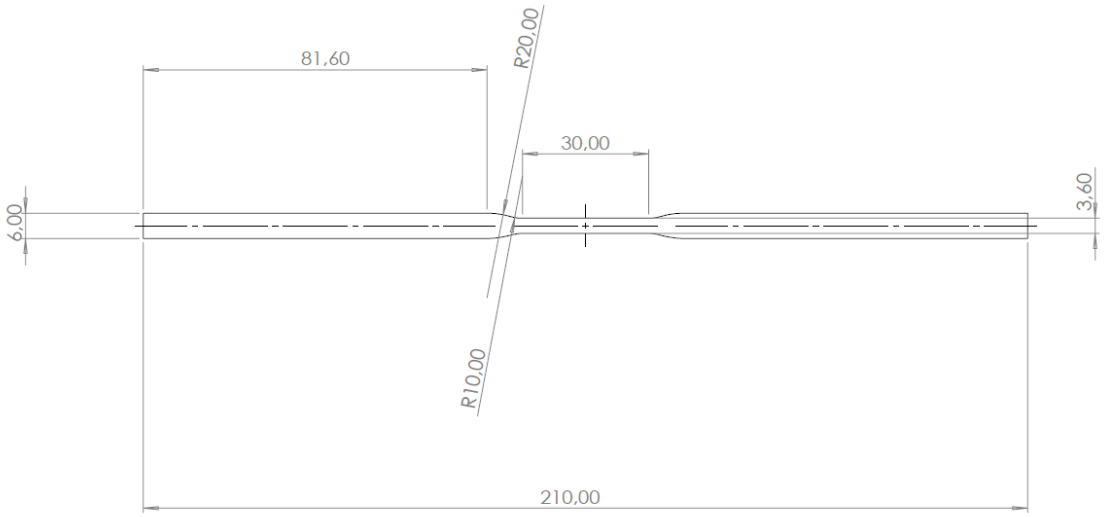

Figure 3.2: *Dog-bone shape laser-cut into the ReBCO samples.*

Laser-cutting was performed using a Lasag-Rofin LFS150 laser, fitted with a LLBK60 Fiber Optic Processing Head. The wavelength is 1000-1200 nm. The laser can emit up to 1500 W pulse power, and 150 W continuous.

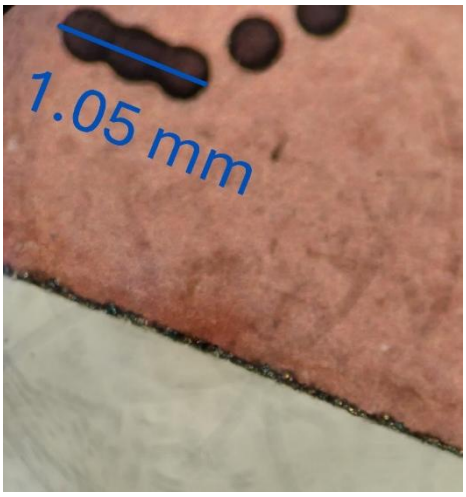

Figure 3.3: Microscope image of lasercut edges of THEVA 230039.

ReBCO samples were clamped into titanium clamps to apply stress and strain. Copper clamps were used to supply current to the tapes. Strain was measured using Nyilas-type extensometers clamped onto the sample using springs. Stress was measured using a Tedea Huntleigh load cell model 614-50kg. A mounted sample is shown in Figure 3.4, showing the copper and titanium clamps, as well as the extensometers and voltage taps. A pair of voltage taps soldered onto the sample within the extensometer arms was connected to a nV amplifier and used to determine critical current.

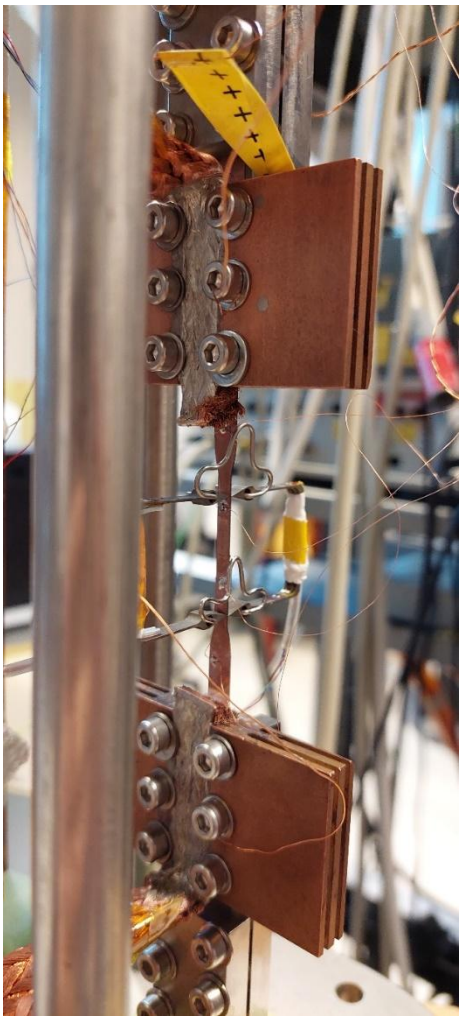

Figure 3.4: *A dog-bone shaped ReBCO sample mounted in the TARSIS facility.*

The cross-sectional area of the lasercut section of the tapes was determined by multiplying the width and thickness as measured using a micrometer. A microscope picture of the lasercut edges is shown in **Erreur ! Source du renvoi introuvable.**.

To determine the $\sigma(\varepsilon)$ curve of samples, a displacement was applied to the top titanium clamp, and stress and strain on the tape were measured. Experiments were performed in a liquid nitrogen bath.

To determine the J_c value as a function of σ and ε, the critical current is measured at various levels of stress and strain. I_c is determined by stepwise increase the current in the sample using a current source, and measuring the voltage over the sample. I_c then corresponds to the current that causes the voltage to exceed the chosen critical electric field value of 100 µV/m.

The $I_c(\varepsilon,\sigma)$ experiment is executed as follows. First, a displacement is applied until σ reaches a given value, e.g. 140 MPa. The displacement is then kept constant while I_c is determined, and then decreased again until σ reaches 5 MPa. At that point, I_c is measured again. The displacement is then again increased until σ reaches its next chosen value, and so on. This process continues until the critical current is significantly degraded. The irreversible stress and strain limits, σ_{irr} and ε_{irr}, are determined from the I_c data at 5 MPa. When I_c at 5 MPa is significantly decreased compared to its original value in the virgin sample, the previously applied stress has caused irreversible degradation. σ_{irr} and ε_{irr} are then determined as the

stress and strain levels where I_c is 99% of its virgin value, using a linear interpolation between the two last stress and strain levels.

To reduce side effects of cycling loading and to keep the measurement time reasonable, the stress level was initially increased in large steps of 140 MPa. σ_{irr} is expected to be approximately linearly related to the yield stress Rp0.2. Therefore, when approximately 75% of the estimated Rp0.2 value for a given sample was reached, smaller steps of 35 MPa were taken.

3.3 Results

3.3.1 Stress-strain

Table 3.1 shows once more the measured young's modulus *E* and the yield stress Rp0.2 of the tested samples. Rp0.2 offset yield stress is defined as the stress where the plastic elongation of the sample is 0.2%. Plastic deformation begins at a lower stress.

It should be noted that the stress/strain curves for THEVA 230039, THEVA 240019, SSTC 2311-351 and SSTC 2402-1911 were determined on the same sample used for determining $I_c(\varepsilon,\sigma)$. The samples had therefore previously been strained up to 0.5%, which may affect the results.

The estimated uncertainty in Rp0.2 stress is 4% of value. The estimated uncertainty in Young's modulus is 6% of value. The error is dominated by the uncertainty in cross sectional area of the sample tapes. [3]

Table 3.2: *Young's modulus and Rp0.2 stress of the tested samples.*

Sample	E [GPa]	Rp0.2 stress [MPa]
THEVA 220057	191	1060
THEVA 230039	193	1155
THEVA 240019	189	1077
Fujikura 22-0197-03	147	786
SSTC 2311-351	180	1161
SSTC 2402-1911	177	974

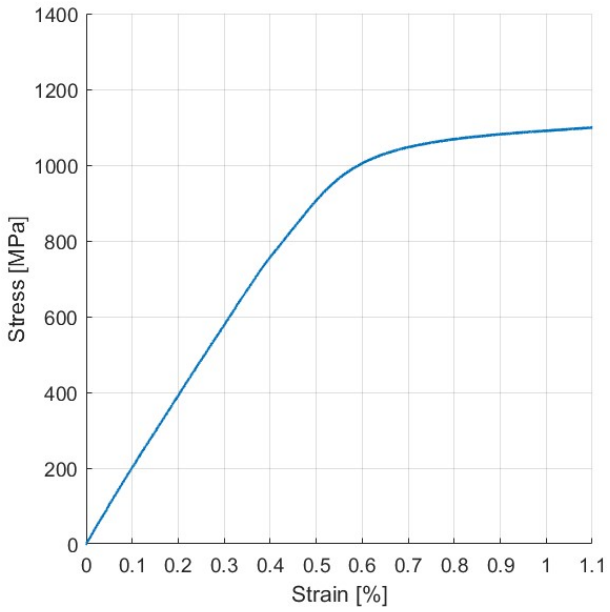

Figure 3.5: Stress/Strain curve of THEVA 220057 at 77 K.

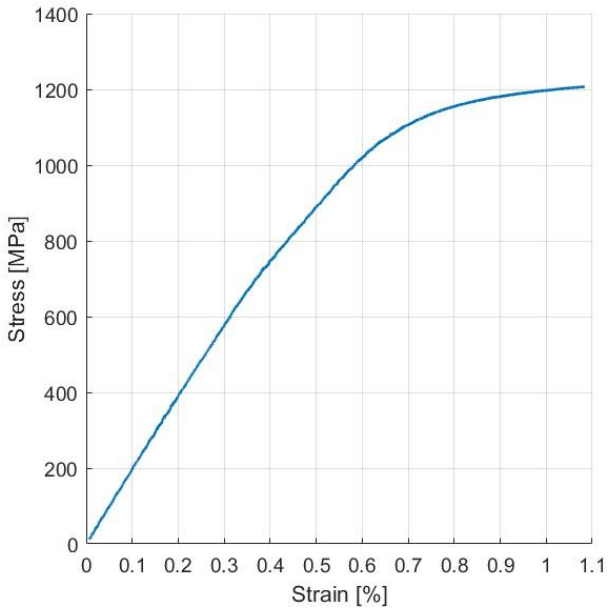

Figure 3.6: Stress/Strain curve of THEVA 230039 at 77 K.

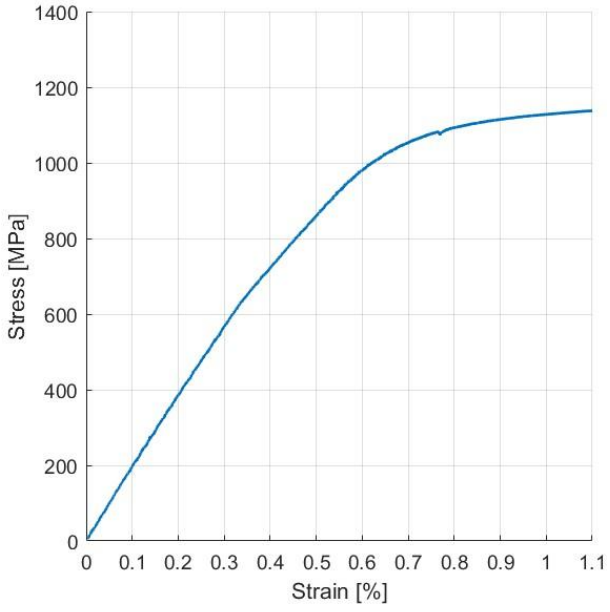

Figure 3.7: Stress/Strain curve of THEVA 240019 at 77 K.

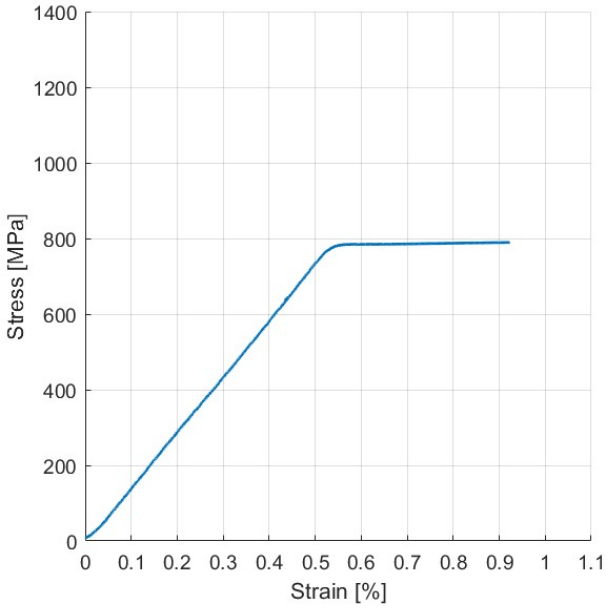

Figure 3.8: Stress/Strain curve Fujikura 22-0197-03 at 77 K.

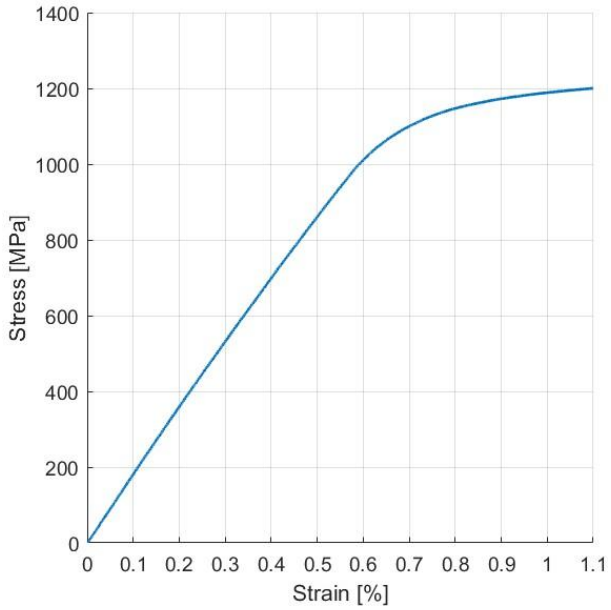

Figure 3.9: Stress/Strain curve SSTC 2311-351 at 77 K.

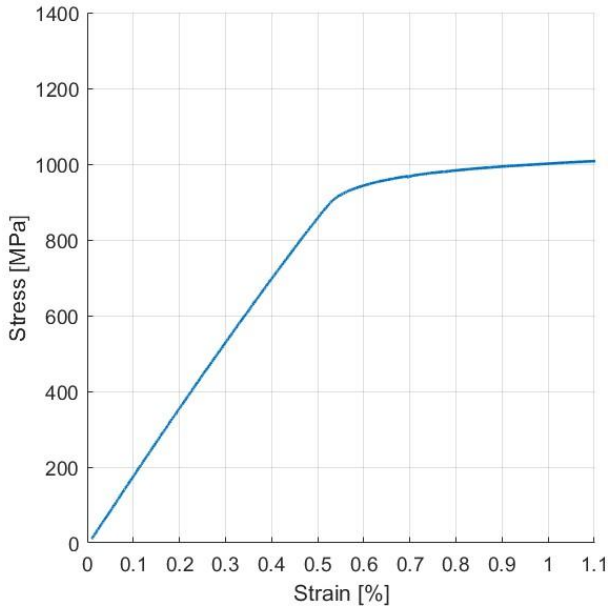

Figure 3.10: Stress/Strain curve SSTC 2402-1911 at 77 K.

3.3.2 Strain sensitivity critical current density

Erreur ! Source du renvoi introuvable..3 shows the overview of the 6 samples measured and their engineering critical current density (critical current over total cross-section of the tape), *n*-value, irreversible strain limit, and irreversible stress limit.

Table 3.3: *Un-strained critical current density and n-value; irreversible stress and strain limits for the tested samples.*

Sample	J_c [A/mm^2]	n-value [-]	ε_{irr} [%]	σ_{irr} [MPa]
THEVA 220057[3]	430	26	n.a.	n.a.
THEVA 230039[4]	523	35	0.28	440
THEVA 240019	421	33	0.29	500
Fujikura 22-0197-03[5]	676	28	0.39	570
SSTC 2311-351	599	34	0.42	680
SSTC 2402-1911	639	34	0.36	570

No irreversibility limits were measured for THEVA 220057. This tape was measured before deciding to cut the tapes to a dog-bone shape, and would quench near the current leads before reaching a nonzero electric field over the voltage taps.

As can be seen when comparing **Erreur ! Source du renvoi introuvable.** and Table 3.1, the I_c of THEVA 230039 started to degrade well below the yield stress. Since this came as a surprise, relatively large load steps were still being taken, meaning the determined σ_{irr} and ε_{irr} of THEVA 230039 have a large uncertainty.

[3] Tape degraded during a quench near current leads at elevated loads, rendering further determination of I_c impossible.
[4] Relatively high uncertainty in ε_{irr} and σ_{irr} values, due to larger stress steps.
[5] Stress data taken from logbook, strain data calculated from logbook values and stress/strain curve.

Due to a software error, stress and strain data was not saved during the $I_c(\varepsilon,\sigma)$ experiment for Fujikura 22-0197-03. Stress data was instead taken from the experiment logbook, where values were rounded to the nearest multiple of 20. This means an additional error of ±10 MPa is present in stress values for this tape. Strain values were calculated using the logbook values and the stress/strain curve of Fujikura 22-0197-03, that was measured on a fresh sample. These strain values too should be viewed only as indication.

Uncertainties in strain values are estimated to be around 10% of value. Uncertainties in stress values are estimated to be around 4%. [3]

Results for THEVA irreversible strain limits are comparable to those reported in [4], Fujikura irreversible strain limit is comparable to that reported in [3] supporting the result reliability. SSTC irreversible strain limits differ from those reported in [3] however. Whether this difference is caused by a difference in tape architecture, or caused by the laser-cutting to create a dog-bone shape is presently still unknown.

In the figures of I_c as a function of stress and strain below, triangles represent the I_c value measured at the given stress/strain level, circles symbolize represent the I_c value measured when the sample is subsequently brought back to 5 MPa. As expected from literature, all tested tapes display a *reversible* reduction of the critical current under load (related to electronic effects) before *irreversible* degradation (related to microstructural damage) sets in.

Erreur ! Source du renvoi introuvable. shows two datasets at 0.31% strain. A double loading-unloading cycle was performed at the same stress/strain level to check if the effect of cyclic loading on the irreversible I_c degradation is low. This is indeed the case.

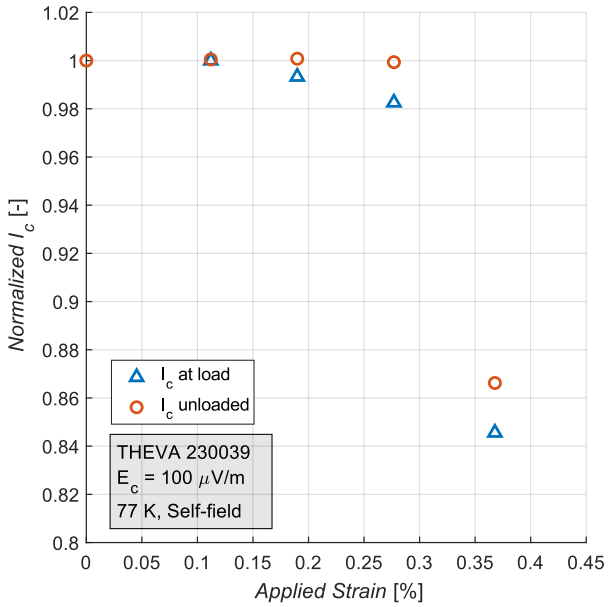

Figure 3.11: I_c vs applied strain for THEVA 230039.

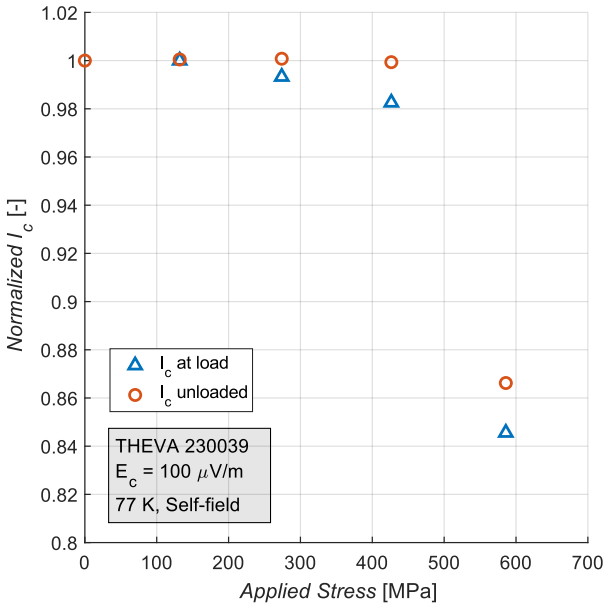

Figure 3.12: I_c vs applied stress for THEVA 230039.

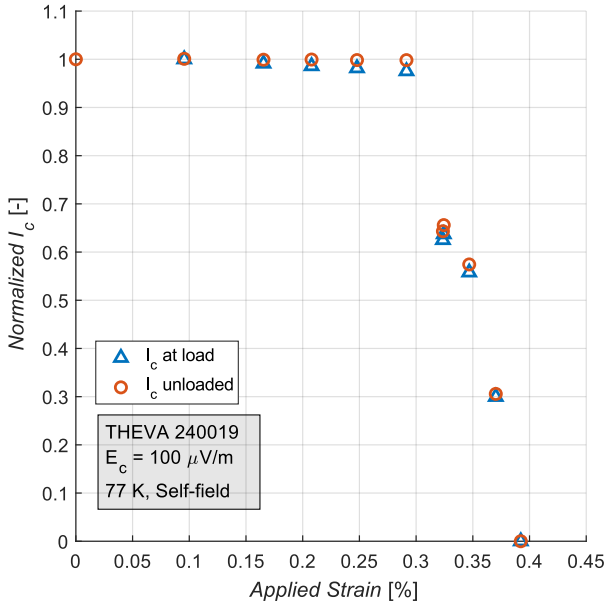

Figure 3.13: I_c vs applied strain for THEVA 240019.

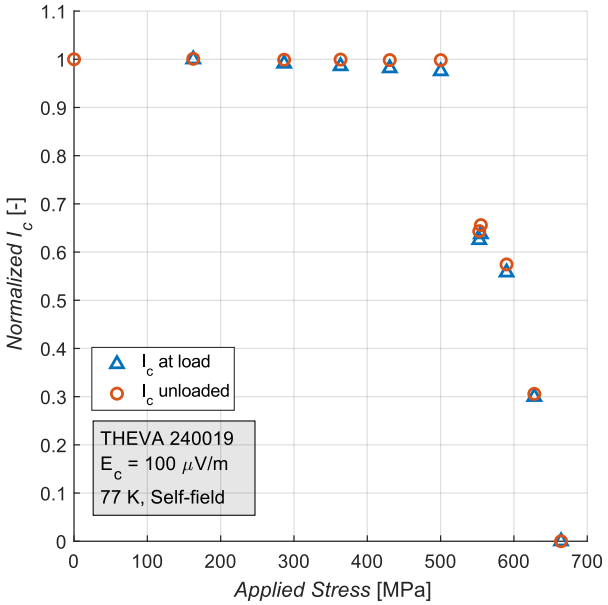

Figure 3.14: I_c vs applied stress for THEVA 240019.

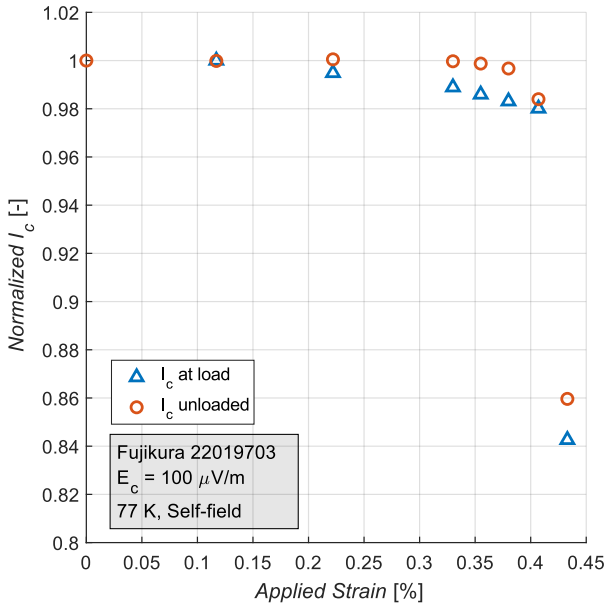

Figure 3.15: I_c vs applied strain for Fujikura 22-0197-03.

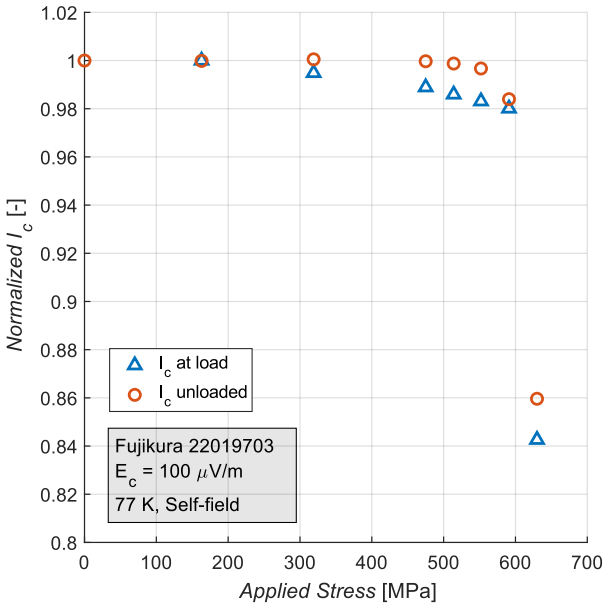

Figure 3.16: I_c vs applied stress for Fujikura 22-0197-03.

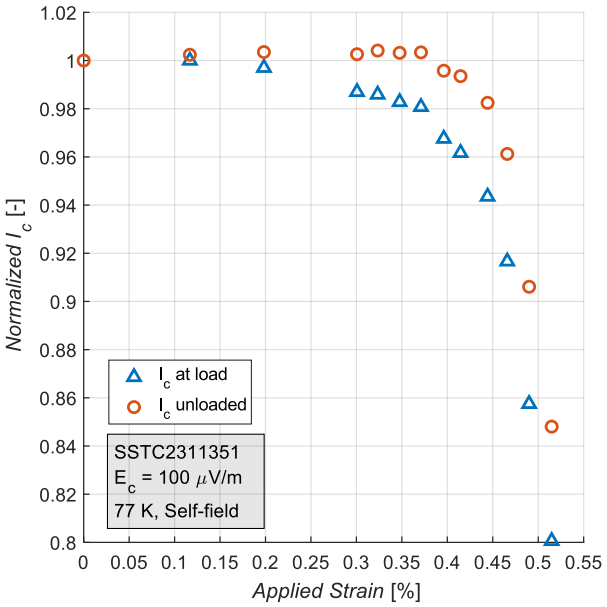

Figure 3.17: I_c vs applied strain for SSTC2311-351.

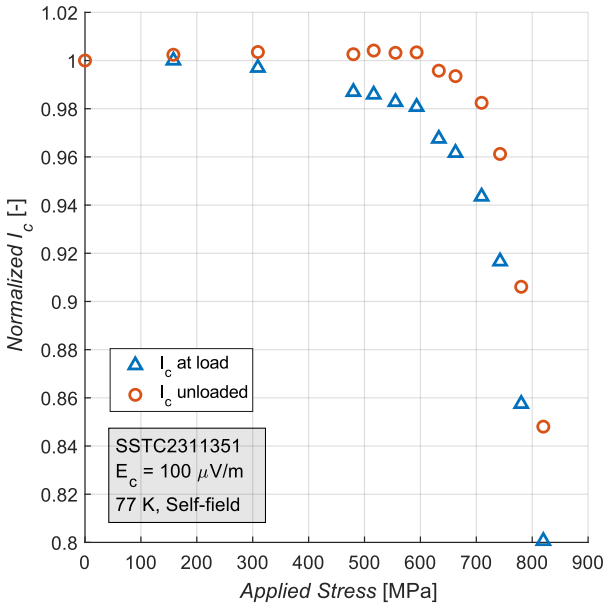

Figure 3.18: I_c vs applied stress for SSTC2311-351.

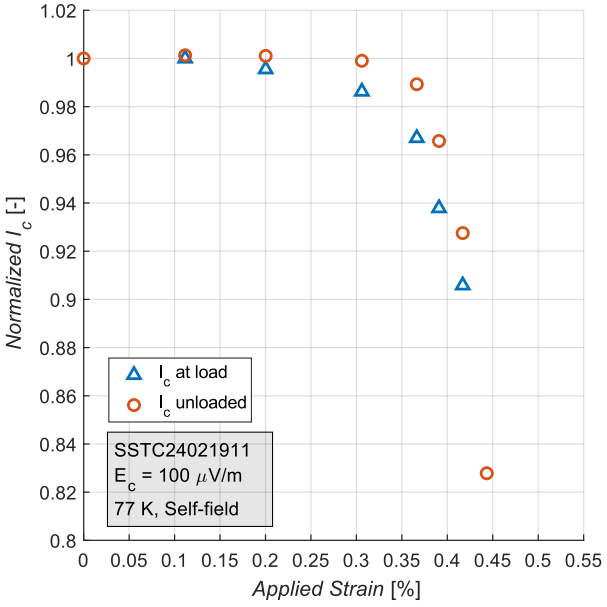

Figure 3.19: I_c vs applied strain for SSTC2402-1911.

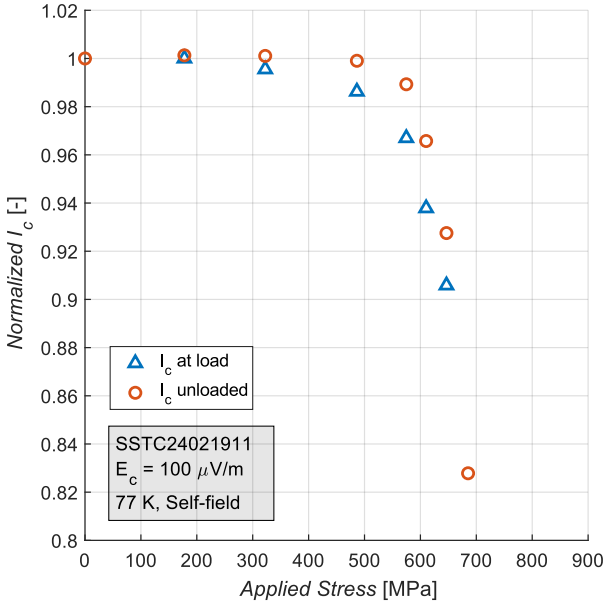

Figure 3.20: I_c vs applied stress for SSTC2402-1911.

4. Sources

[1] H. Zhang *et al.*, "*Database of the effect of stabilizer on the resistivity and thermal conductivity of 20 different commercial REBCO tapes*", Supercond. Sci. Technol. 35 (2022), 045016, March 2022

[2] H. Zhang *et al.*, "*Exploration of correlation between the material characteristics of the copper layer on the electrical and thermal properties of REBCO tape and coil*", Journal of Alloys and Compounds 925 (2022), 166770, August 2022

[3] J. Rietberg, "*Critical current testing of ReBCO tapes under applied axial tensile stress and strain with the new TARSIS setup*", Master Thesis, University of Twente, July 2024

[4] A. Toda *et al.*, "*Influence of tensile damage on V–I curve and critical current of DyBCO coated conductor*", Physica C: Superconductivity and its applications, 470 (2010), 1346-1349, May 2010